Photon-in/photon-out spectroscopy at the I20-scanning beamline at diamond light source

Shusaku Hayama[1], **Roberto Boada**[1,2], **Jesús Chaboy**[1], **Adrian Birt**[1], **Graham Duller**[1], **Leo Cahill**[1], **Adam Freeman**[1], **Monica Amboage**[1], **Luke Keenan**[1] **and Sofia Diaz-Moreno**[1,*]

[1] Diamond Light Source Ltd., Harwell Science and Innovation Campus, Didcot, Oxfordshire OX11 0DE, United Kingdom
[2] Department of Chemistry, Universitat Autònoma de Barcelona, 08193 Bellaterra, Barcelona, Spain

E-mail: sofia.diaz-moreno@diamond.ac.uk

Abstract
A scanning multi-crystal x-ray emission spectrometer to perform photon-in/photon-out spectroscopy at the I20-Scanning beamline at Diamond Light Source is described. The instrument, equipped with three analyzer crystals, is based on a 1 m Rowland circle spectrometer operating in the vertical plane. The energy resolution of the spectrometer is of the order of 1 eV, having sufficient resolving power to overcome the core-hole lifetime broadening of most of the transition metals *K*-edges. Examples showing the capability of the beamline for performing high energy resolution fluorescence detection x-ray absorption spectroscopy (HERFD-XAS), non-resonant x-ray emission spectroscopy (XES) and resonant x-ray emission spectroscopy are presented. The comparison of the Zn and Mn *K*-edge HERFD–XANES of ZnO and MnO with *ab initio* calculations shows that the technique provides enhanced validation of the models by making subtle spectral features more visible.

Keywords: x-ray spectroscopy, photon-in/photon-out spectroscopy, x-ray emission spectroscopy, high energy resolution fluorescence detection x-ray absorption spectroscopy, resonant x-ray emission spectroscopy, HERFD–XANES

(Some figures may appear in colour only in the online journal)

1. Introduction

X-ray absorption spectroscopy (XAS) is an established experimental technique at synchrotron radiation facilities that is used for the study of the electronic and local atomic structure of materials [1–3]. The high sensitivity of the method together with its element selectivity make it possible to undertake experiments targeted on functional chemical sites under realistic conditions of concentration. As XAS is a local structural probe, it is applicable to all states of matter; crystalline or amorphous solids, liquids and gases. These characteristics make the technique suitable for application in many different scientific disciplines, from chemistry and catalysis, to environmental science, materials science, physics, biology, and others.

In recent years, photon-in/photon-out core-level spectroscopy has expanded the x-ray spectroscopy toolkit for investigating chemically specific electronic and geometrical structures [4–6]. By analysing the energy of the scattered/emitted photons with high energy resolution with an energy bandwidth on the order of the core-hole lifetime broadening of the inner-shell electron hole, the range of applications of conventional XAS is increased and some of its shortcomings can be

circumvented [7, 8]. High energy resolution fluorescence detection XAS (HERFD–XAS), non-resonant x-ray emission spectroscopy (XES), and resonant x-ray emission spectroscopy (RXES), also called resonant inelastic x-ray scattering, have been developed hand in hand with the increasing accessibility of efficient x-ray emission spectrometers that cover a large solid angle of detection.

Most x-ray emission spectrometers operating at synchrotron beamlines are based on multiple bent crystal analysers operating under Bragg scattering condition close to back-scattering [9–20]. Point to point scanning spectrometers are usually based on a Rowland circle geometry following the Johann [21] or Johansson [22] schemes, while dispersive spectrometers are usually realized in the von Hamos geometry [23]. In this report, we present a technical description of the multi-analyser scanning hard x-ray emission spectrometer that has been designed and built for the I20-Scanning beamline at Diamond Light Source [24], and illustrate its capabilities with a range of examples. The beamline is particularly well suited to house the emission spectrometer as it makes use of a 2 m wiggler and is equipped with a state-of-the-art four-bounce monochromator which can deliver tuneable, high-brightness and stable hard x-rays to the end-stations [25]. The beamline covers the energy range from 4 to 20 keV. The incident photon flux is $>10^{12}$ photons per second when using the Si(111) monochromator. The design of the I20 emission spectrometer has been optimised for carrying out HERFD–XAS, XES, and RXES maps, and examples of these methods are presented that demonstrate the capabilities of the instrument. In addition, *ab initio* calculations performed at the Zn and Mn K-edges for ZnO and MnO respectively, are compared with the HERFD–XANES spectra, showing the good agreement achieved between experiment and theory after enhancing the experimental sensitivity, and making the assignment of near-edge spectral features much more reliable.

2. Spectrometer design

Most of the point-to-point scanning x-ray emission spectrometers operating at synchrotron beamlines are based on a Johann-type geometry [9–17] and the I20-Scanning spectrometer is no exception. This geometry utilises spherical or cylindrical analyser crystals that are bent to a *radius*, R, to maximise the photon capture efficiency of the spectrometer. All the optical components of the instrument, including the sample, are placed on a Rowland circle of *diameter R* (see figure 1). In this set-up, the analyser crystal(s) will focus and collect photons that are emitted from the sample onto the detector using a symmetric Bragg reflection, selecting photons of wavelength λ for a cubic system:

$$n\lambda = 2\sin(\theta_B)(a/(h^2 + k^2 + l^2)^{1/2}) \qquad (1)$$

where n is an integer, θ_B is the angle between the incoming beam and the diffraction plane on the analyser, a is the lattice parameter, and hkl are the Miller indices of the analyser. This expression is only an approximation for the Johann geometry as strictly speaking, only the centre of the analyser crystal is
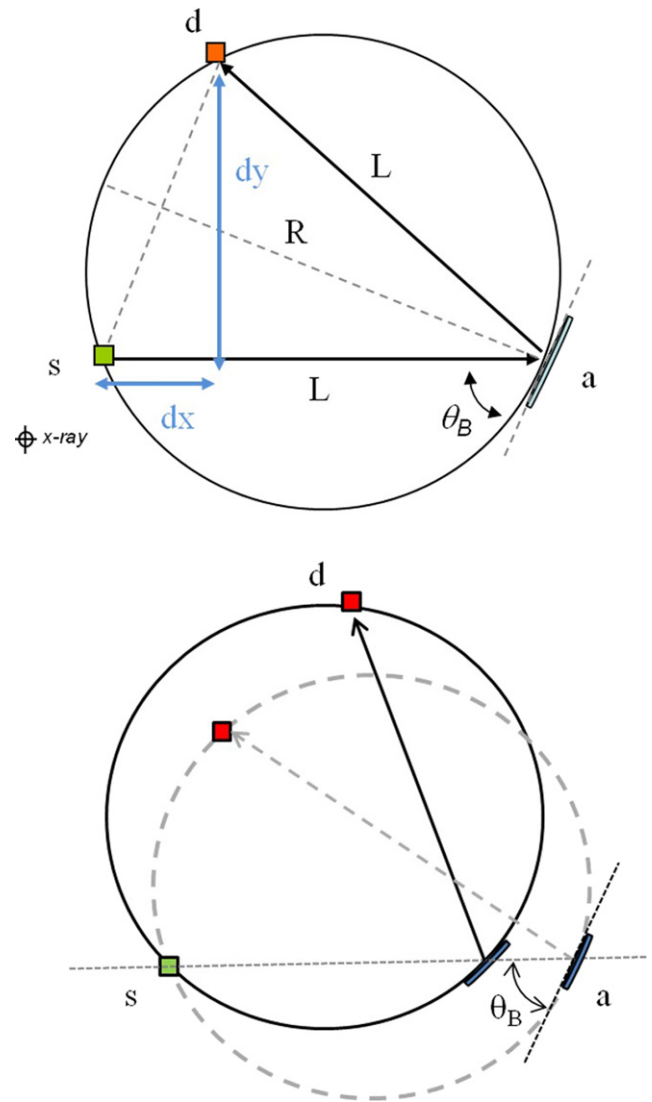

Figure 1. Schematic illustration of the Rowland geometry, where s-sample, a-analyzer, d-detector, L-distance between the sample and analyzer (the analyzer and detector), R-the radius of curvature and dx and dy are the detector x and y positions respectively from s. The sample position is fixed relative to the incident x-ray beam. θ_B is the Bragg angle.

on the circle because the diameter of the Rowland circle is the same as the radius of curvature of the crystal [11, 26]. A number of researchers have demonstrated that the approximation is best satisfied when θ_B is close to backscattering (90°), R is as largest as possible, and the diameter of the analyser crystal is as small as possible [27]. Consequently these parameters must be chosen carefully when designing this type of spectrometer to suit the needs of each beamline.

The I20 spectrometer has a 1 m fixed diameter Rowland circle and uses analyser crystals of 100 mm diameter. The spectrometer is currently equipped with three analyser crystals. The option of increasing the diameter of the Rowland circle to 2 m to enhance the overall spectral resolution of the instrument was considered at the conceptual design stage of the spectrometer. However, the 2 m design was discarded due to the four-fold reduction in the collected solid angle,
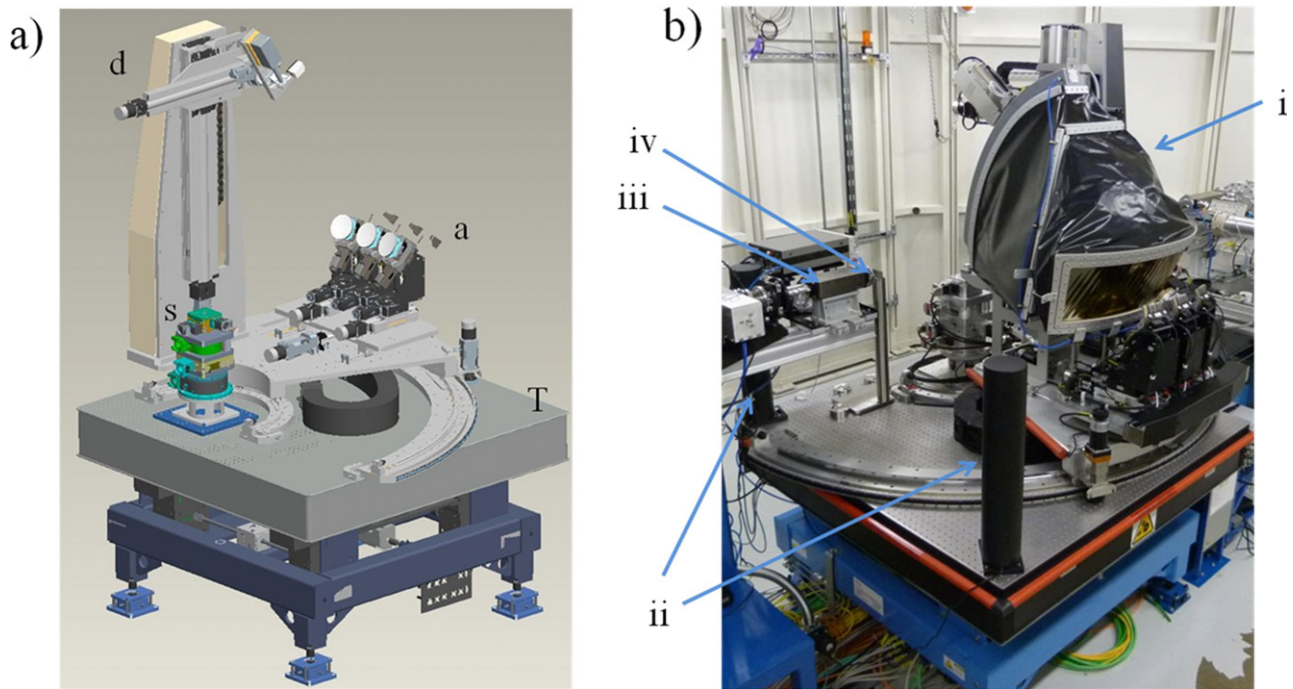
Figure 2. (a) Mechanical design of the I20 XES spectrometer: s-in-house sample stages, a-analyzer assembly, d-detector assembly and T-experimental table. The illustration is only showing the spectrometer at 90° to the incoming beam but can be rotated around the sample position. (b) Photo of the spectrometer: (i) helium bag, (ii) crosshair lasers, (iii) ion chamber and (iv) master aperture at the upstream position (only used for alignment). The origin of the spectrometer is located at 57.025 m from the source.

~0.016% instead of the ~0.063% for a 100 mm diameter analyser crystal at 1 m. Furthermore, in the 2 m design it would not be possible to take full advantage of the larger circle due to the intrinsic resolution restrictions imposed by the spectral purity of the incident beam. In the case of I20, the four-bounce monochromator is equipped with Si(111) crystals, and, although the dispersive configuration ensures that the incident energy resolution is maintained regardless of the configuration of the upstream optics, it makes a significant contribution on the overal resolution of the experiment.

The geometry of the Rowland circle is another important aspect that governs the total resolution of the spectrometer as demonstrated by Bergmann *et al* [27]. They have shown that the source-size at the sample position is a very important factor and should be minimised to achieve the highest spectral resolution. The Rowland circle of the I20 spectrometer has therefore been implemented in the vertical operating plane to benefit from the smaller vertical source size; the beam-size at the sample position is 400 μm (h) $\times$ 300 μm (v) FWHM. Choosing a vertical Rowland geometry also eliminates any dependency on the sample orientation: in typical emission experiments, the sample is oriented at 45° in the horizontal plane with respect to the incident beam to keep the analyser and detector perpendicular to the incoming beam. In the case of a horizontal configuration, the horizontal source-size seen by the analyser/detector would increase with increasing beam-sample angle, essentially making an undesireable geometrical contribution to the energy resolution that is dependent on the experimental set-up and sample alignment.

The mechanical design of the hard x-ray I20-Scanning emission spectrometer is illustrated in figure 2. The spectrometer was designed, assembled and commissioned in-house and is permanently mounted on a dedicated optical table (1.4 m $\times$ 1.4 m) in the experimental hutch of the I20-Scanning beamline. This set-up ensures that the accurate positioning of the analyser crystals and the detector around the x-ray beam source position (sample) is always maintained. The optical table is motorised, and the entire spectrometer can be moved in the vertical plane and in the perpendicular direction to the incoming beam. We note that the sample position is the only fixed point of the instrument and acts as the origin of the spectrometer. On top of this table, there is a rotational motorised base-plate upon which all the components of the spectrometer are mounted. The motorised rotational movement, *main_rot*, is provided to allow the instrument to be moved around the sample position (−10 to +58°, taken the 0° as the position when spectrometer is in a perpendicular position to the x-ray beam) in the horizontal plane while maintaining the Rowland alignment between the analyser crystals and the detector in the vertical plane. This motion greatly improves the flexibility of the spectrometer by making it possible to accept a wider range of sample environments by not limiting the incident beam-spectrometer angle to 90°.

In order to put the centre of the analyser surface on the desired Rowland coordinates, each analyser crystal is mounted on a motorised stage assembly consisting of tilt, lift (*y*-axis) and pitch stages. The central analyser which lies along the *x*-axis when *main_rot* = 0° acts as a master for the other side analysers (minus and plus) and defines the diameter of the
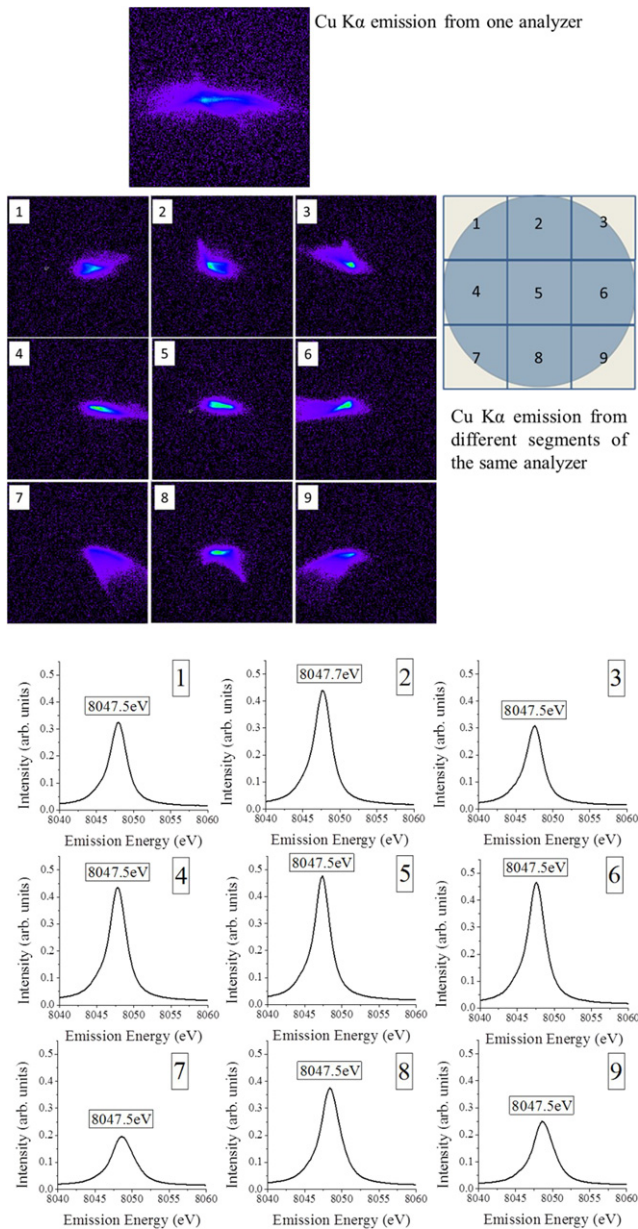
Figure 3. Images captured by the Medipix detector from one Si(111) analyzer crystal. All the images were taken at the maximum of the Cu $K_{\alpha 1}$ emission peak using the Si(444) reflection with the spectrometer at ∼79.3°. To evaluate the quality of this analyzer crystal, a square mask was placed in the front of the analyzer to check the focus quality and spectral shape from nine separate segments. These measurements show the bottom-edge of this analyzer crystal is affected by non-uniform strain and masking this small region of the crystal can greatly improve the energy-resolution from this analyzer.

Figure 4. Current list of the analyzer crystals that are available at I20 and the energy range covered by each crystal orientation.

Figure 5. Spectra of elastically scattered photons measured with one Si(444) analyser crystal with a 90 mm diameter circular mask in the front. The spectrometer was set at 79.3° and 84° for (a) and (b) respectively. The quality of the focus improves significantly when close to backscattering. The FWHM of the elastic peak is ∼1.3 eV and ∼1.0 eV for (a) and (b) respectively.

Rowland circle, R. A decision has also been made to fix the central analyser at the same height as the sample position when scanning the spectrometer. The analyser stages are mounted on a large translation platform, with the central analyser assembly fixed to this stage. To change the Bragg angle of the central analyser, it is only necessary to translate using this stage and pitch towards the detector (see figure 1). The plus and minus analysers are located at ±137 mm from the centre analyser, and are equipped with additional short-range translation stages to move them along the x-axis with respect to the central anal-
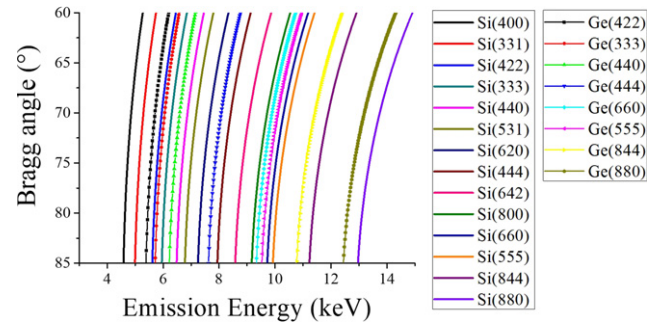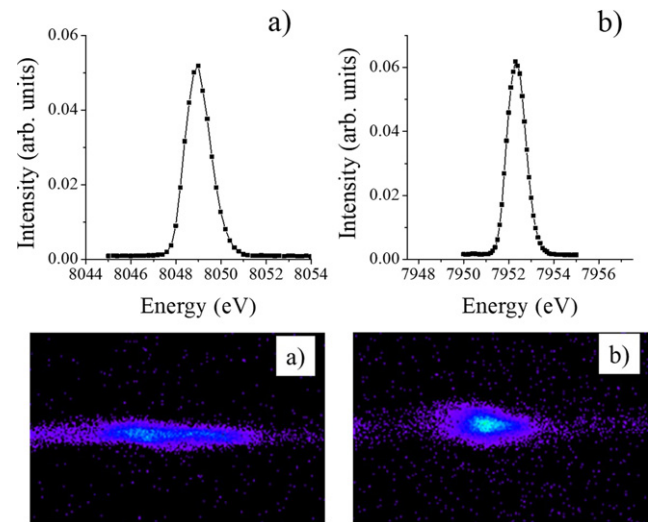
yser. The Rowland circles for the plus and minus analysers are off-centre from the plane of the central Rowland circle, and must be tilted and moved in the horizontal direction as well as in the vertical direction relative to the central analyser to maintain the Rowland condition. All the analyser stages, apart from the tilt stages, are equipped with an encoder and each stage has enough resolution to allow a step-size of 0.2 eV.

The detector movement must follow a large circular-arc, pointing towards the analyser crystals and is placed at the focal point to maintain the Rowland condition. The detector is mounted on a small rotary goniometer via a detachable adaptor plate. A set of motorized slits are available and can be mounted in front of the detector when it is necessary to minimize the background signal. The detector assembly is carried by a highly rigid x–y axis positioning structure which is located on the main rotating platform. The detector position in x and y coordinates relative to the sample position (dx.dy) is shown in figure 1. Currently, the spectrometer is operated in the energy range from 4.5 to 18 keV, and it can be equipped with either a one-element Si-drift detector
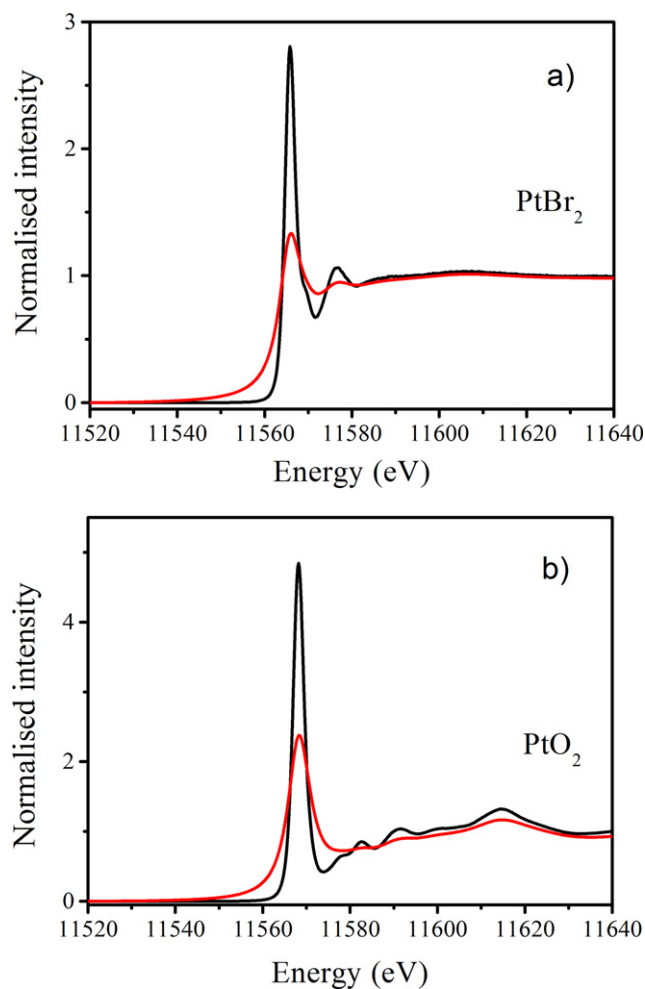
Figure 6. Comparison between normalised HERFD–XANES (black line) and normalised conventional XANES spectra for $PtBr_2$ and PtO_2.

Figure 7. (a) $L_{\alpha 1}$ and $L_{\alpha 2}$ emission lines of a platinum foil. The measured FWHM of the $L_{\alpha 1}$ is 4.2 ± 0.2 eV. (b) HERFD–XANES spectra collected at the $L_{\alpha 1}$ emission line. 60 consecutive scans are shown, demonstrating the excellent reproducibility of the measurements. Each scan was collected in 15 min to obtain a good signal to noise ratio.

(SII Nanotechnology) or a Medipix-Merlin photon-counting pixel detector. The Si-drift detector is mainly used to perform experiments below 4.8 keV, as well as in those cases when there is a need to discriminate unwanted photons selected by other harmonics of the analyser crystals (for example, to reject the La $L\gamma_1$, 5785.7 eV, from Ge(333) when collecting Co $K_{\beta 2,5}$, 7706 eV, from Ge(444) in $LaCoO_3$). The Medipix detector is a high performance x-ray imaging detector that has been developed at Diamond Light Source [28]. The active area of this detector is 14 mm × 14 mm with 55 μm pixel size and it offers a 12 bit dynamic range per pixel with the possibility of selecting a region of pixels to be acquired. A few examples of images taken with this detector are shown in figure 3. Because a pixel detector is capable of directly imaging the secondary photons, it can be readily used to check the focus-quality and radius of curvature of each analyser crystal by simply looking at the shape and size of the image that is being collected. Furthermore, it was found that the Medipix detector is especially useful when aligning more than one analyser crystal. A better alignment with an improved spectral resolution is achieved having access to the beam image rather than sim-
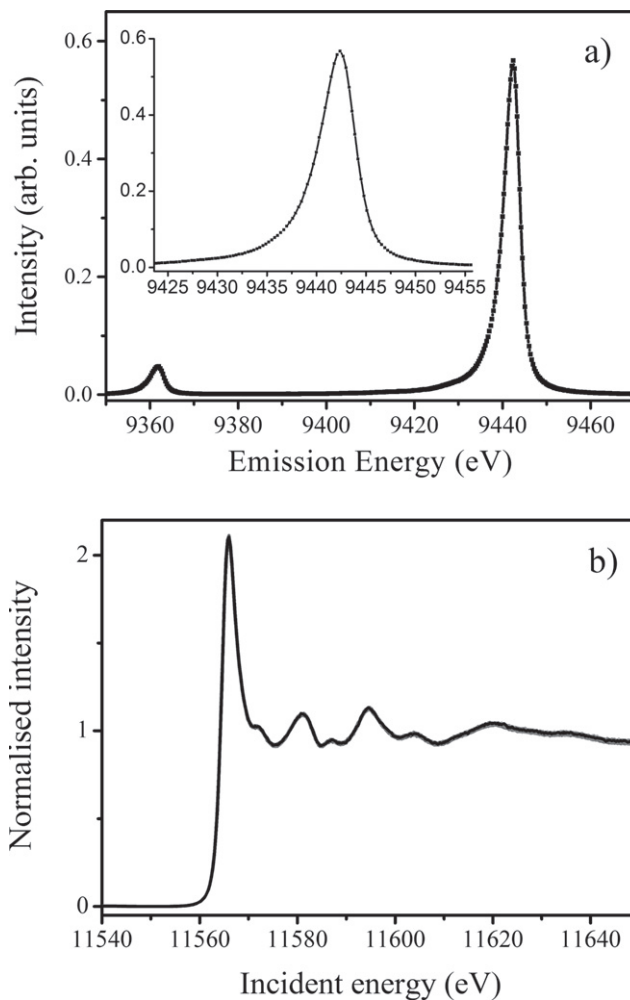
ply maximizing the count rate as with the Si-drift detector. Recently, a four element Medipix detector has been acquired for the beamline (14 mm × 56 mm). The wider version is particularly useful when operating the spectrometer below 78°, when the horizontal size of the focal spot at the detector becomes too large to be captured with the single-element detector. In addition, the use of the larger detector offers the possibility of collecting the beam from each analyser crystal independently.

Although the angular range of the spectrometer, θ_B, has been designed to cover the range from 85° to 60°, it is preferable to use the spectrometer in a near-backscattering configuration with Bragg angles as close to 90° as possible [26]. To help facilitate this, a battery of spherically-bent silicon and germanium analyser crystals with different crystal cuts that can operate at multiple orders of reflection (*hkl*) has been made available (see figure 4).These crystal sets cover most of the K_α and K_β emission lines of the first row transition metals. In recent years, strip-bent analyser crystals have

Figure 9. PrBr$_2$ HERFD–EXAFS taken with three Ge(660) analyser crystals and conventional EXAFS spectra taken in transmission mode (black lines) and best fit (red lines) performed using the Demeter software [48] and following standard procedures. The acquisition times for transmission and HERFD–EXAFS are approximately 20 and 80 min, respectively.
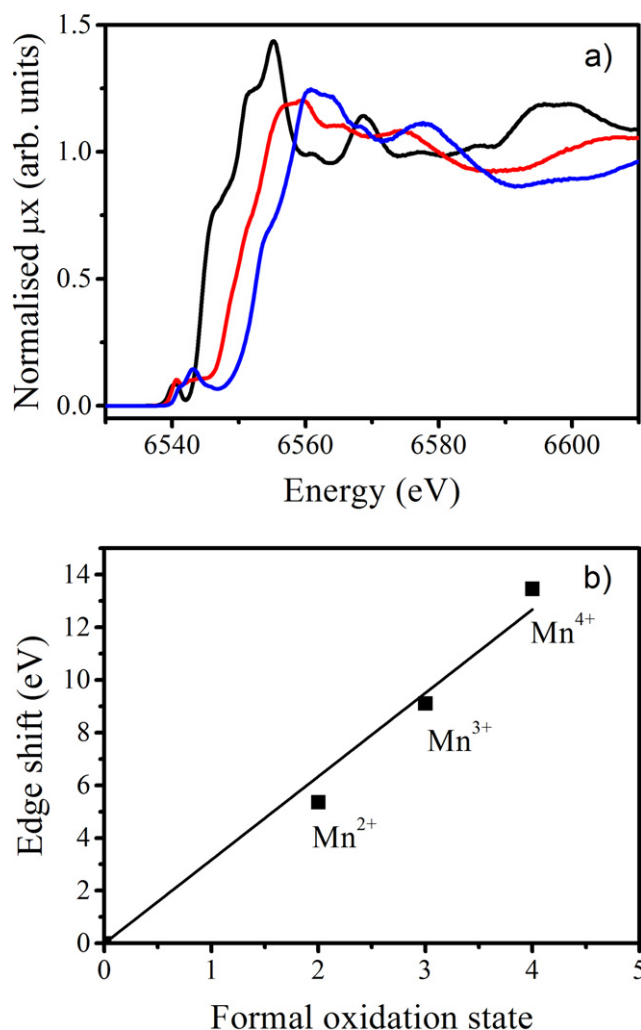

Figure 8. (a) Normalised HERFD–XANES spectra for MnO (black line), Mn$_2$O$_3$ (red line) and MnO$_2$ (blue line). (b) The edge positions, taken as the maximum of the first derivative) are plotted as a function of the formal oxidation state with the Mn foil edge position (6539 eV) at the origin.

become commercially available [29], providing a smaller focus and improved energy-resolution than the single-wafer type crystals, thanks to the reduced strain [30].

Finally, the spectrometer is equipped with a helium-filled bag that is placed between the sample position, the analyser crystals and the detector to minimise the air path (figure 2(b) shows a photograph of the spectrometer with the helium-bag in place). The helium bag is constructed from a rigid structure and two large kapton windows (25 μm thickness) and it can be used for the entire operational range of the spectrometer. The use of a helium environment is essential as the absorption coefficient of air is not negligible in the working energy range of the spectrometer. For example, at 10 keV, the absorption coefficient of air is 0.005 9 cm^{-1}, hence only $\sim$30% of photons are transmitted through 200 cm of air. At 5 keV, almost all the photons are lost as the absorption coefficient of air increases to 0.048 cm^{-1}.
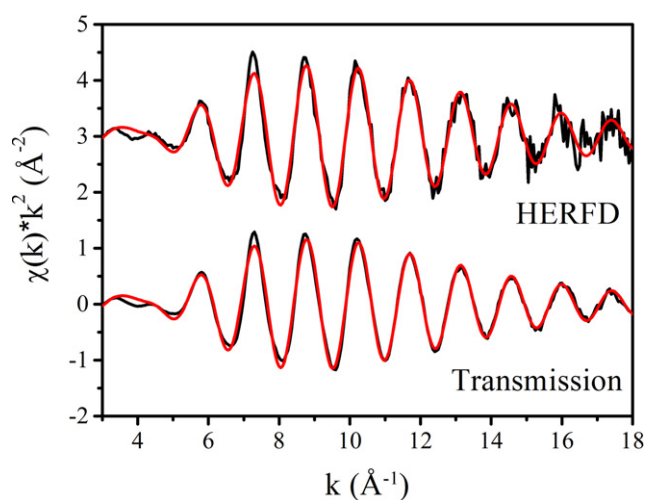
2.1. Spectrometer alignment

The alignment of the XES spectrometer is performed in three stages. The first step uses a laser tracker (Leica Absolute Tracker) to accurately place the analyser crystals and the detector to a known position and set the position of each stage relative to the origin of the spectrometer. In the case of the analyser stages, this was done at the backscattering geometry, $\theta_B = 90°$, adjusting the stages until the centre of the analyser surface was located at the same height and translated 1000 mm from the sample position. The offset in the analyser stages was then set so that the current readback values were consistent with the $\theta_B = 90°$ positions. The pitch and tilt analyser stages were then set to the $\theta_B = 90°$ position using a high-precision square spirit level. The laser tracker and a small reflector were also used to identify the centre of rotation of the detector and the main horizontal rotation stages.

The next step of alignment is achieved using a set of laser-alignment tools especially developed for the spectrometer. The alignment tools consist of a master aperture, secondary aperture with a laser, and two crosshair lasers (figure 2(b)). The master aperture has a fixed pin-hole of 0.8 mm diameter and is designed so that it can be accurately located at two positions: (i) with the aperture at the sample position and (ii) just upstream of this position with the pin-hole aligned with the sample position. The master aperture is predominantly used in the upstream position for aligning the origin of the spectrometer to the incident x-ray beam by adjusting the optical table (x and y) until the incident beam is at the centre of the pin-hole. The two cross-hair lasers are permanently mounted at the upstream corners of the optical table and the intersection of their crosshairs is used to identify the position of the sample. The secondary aperture laser system is adjustable and used for aligning the analyser crystals and detector by shining the laser
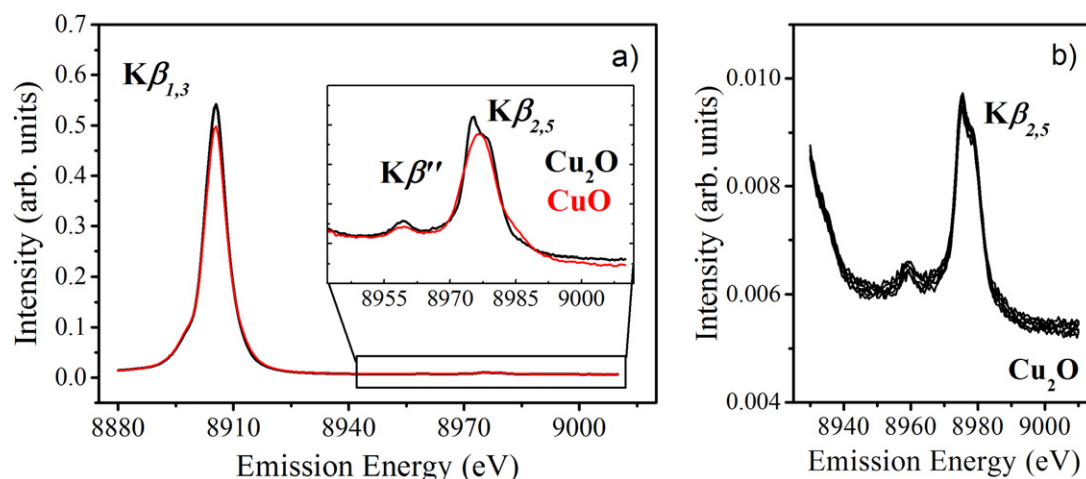
Figure 10. (a) K_β XES for Cu_2O and CuO. The intensity of the $K_{\beta 2,5}$ line is very weak, only about 1.5% of the main $K_{\beta 1,3}$ line; (b) six consecutives scans (8 s per point) taken from the Cu_2O samples in the satellite region.

on the crystal surface and checking the position of the reflected beam at the detector. If necessary, small manual adjustments (tilt, *x* and *y*) of each analyser holder and/or the detector stages are carried out in order to place the reflected beam on the centre of the detector to satisfy the Rowland condition. Typically this process is repeated at two Bragg positions to confirm that the linearity of the spectrometer is maintained within the measurement range of interest. It should also be noted that the secondary aperture system is carefully aligned to ensure the laser beam overlays the path of emitted photons as closely as possible. This is done by ensuring that the secondary aperture is at the sample position using the crosshairs of the upstream lasers and simultaneously passing the secondary laser beam through the master aperture located at its upstream position to make the laser beam parallel with the horizontal plane.

The final step of alignment is done with x-rays to correct for any small mismatch (e.g. miscut of the crystal) between the laser and x-ray positions by simply finding the peak of the chosen emission line from a metal foil with the beamline monochromator set between 100 eV to 200 eV above the absorption edge. When more than one analyser crystal is used, each is aligned separately to ensure that the energy calibration and linearity of the emission spectra are consistent from one analyser to the other. We note that only minor adjustments to the tilt and pitch of the analyser stages are typically needed to find the emission line at the detector. Once the spectrometer is aligned, the peak of the main emission line (or elastically scattered peak) is recorded and the energy of the spectrometer is calibrated to the tabulated value [31]. If the Medipix detector is in use, the diameter of the Rowland circle, *R*, is also tweaked until the best focus and energy-resolution are attained. The second and third steps described above are always repeated when the spectrometer is reconfigured to measure different emission lines.

3. Spectrometer capabilities

The overall energy resolution of the spectrometer is variable and difficult to calculate accurately as it depends greatly on the spectrometer geometry and the quality of analyser crystals, but it can be routinely estimated by measuring the width of an elastic scattering peak once the upstream optics and the spectrometer is configured for a specific emission line. Figure 5 shows the emission spectra of elastically scattered photons from a vitreous carbon foil measured using the XES spectrometer at two different angles. The spectra were acquired using the Si(111) monochromator that has been calibrated at the Cu *K*-edge and one Si(444) analyser crystal, mounted on the central analyser position. The incident intensity was simultaneously measured using an 15 cm long ion chamber (OKEN) and the position sensitive Medipix detector was used to measure the emitted photons. As expected, the resolution improves significantly when the spectrometer is rotated from 79.3° to 84°, as the geometrical contributions to the energy resolution are minimized the closer to backscattering geometry the spectrometer operates. Since the measured energy resolution can be estimated as a convolution of the incident and spectrometer resolutions, and the intrinsic resolution of the Si(111) monochromator is about 1.0 eV at 8 keV, we can estimate that the energy resolution of the spectrometer equipped with the Si(444) analyser is of the order of 0.8 eV at the Cu K_α-line energy (8047.8 eV, 79.3°). Although this is an estimate only as the measured line shape is neither totally symmetric nor Gaussian-like, it still demonstrates that the inherent resolution of the I20 spectrometer is remarkably good.

To demonstrate the capabilities of the emission spectrometer, three different types of experiments are described below.

3.1. High energy resolution fluorescence detection XAS

HERFD–XAS data is collected by aligning the spectrometer to the maximum of the emission line of interest, while the incident energy is scanned through the absorption edge (XANES) and/or over the extended energy region (EXAFS). The intensity variation of the emitted line is recorded as a function of the incident energy.

Figure 6 shows a comparison between the HERFD –XANES spectra and the conventional XANES spectra collected in transmission mode on the same platinum containing samples. The high-energy resolution spectra were obtained
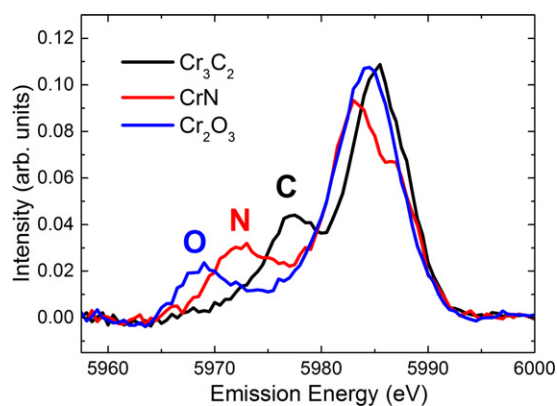
Figure 11. V2C–XES for Cr_3C_2, CrN and Cr_2O_3. The energy position of the K_β'' emission line is given by the nature of the ligand bond to the chromium centre.

using three Ge(660) analyser crystals with the spectrometer fixed at the Pt $L_{\alpha1}$ emission line and scanning the incident energy across the Pt L_3-edge. To check the energy calibration of the spectrometer, the emission line of a platinum metal foil (Goodfellow, 5 μm thickness) was measured with the incident energy set well-above the Pt L_3 absorption edge (11 564 eV). The measured $L_{\alpha1}$ and $L_{\alpha2}$ emission energies and the line shape of the $L_{\alpha1}$ emission line (see figure 7) verify that the linearity and calibration of the spectrometer are excellent in the measurement range. We have also checked the reproducibility of the HERFD–XANES scans by repeatedly taking the same spectra with the XES spectrometer positioned at the peak of the measured $L_{\alpha1}$ emission line (9442.3 eV, $\theta_B = 79.93°$) using three analyser crystals. We see that the edge features are extremely reproducible with no visible change in the edge position over a time span of 14 h, and these scans can be safely merged without additional alignment of the energy scale. The features in the edge region measured with the spectrometer are sharper and better defined than when measured using conventional XANES, due to the capability of the measurements taken with the spectrometer to overcome the core-hole lifetime broadening [7]. This capability makes the task of assigning a particular feature of the near-edge much more reliable and offers new insight into qualitative or fingerprinting interpretations of the XANES structures. Furthermore, the spectrometer can be used to probe a specific decay-channel in the edge region by tuning to a particular emission line of interest, providing yet another powerful tool for studying the electronic/spin states of matter.

The XANES region of the absorption spectrum is sensitive to the electronic structure and local geometry around the absorbing atom [1–3]. The energy shift of the absorption threshold is related to the oxidation state of the absorber through the modification of the next-neighbouring interatomic distances and, consequently, the edge position is very often used to determine formal oxidation states [32–34]. Figure 8 shows a set of K-edge HERFD–XANES of a series of manganese oxides. These spectra were collected using one Si(422) analyser crystal with the spectrometer fixed at the Mn $K_{\alpha1}$ line (5898.75 eV). As shown in the figure, the edge position of the spectra (determined as the maximum of the first derivative of

the XANES) shifts to higher energy with increasing oxidation state of the manganese centre, as was already shown by Zaharieva *et al* using conventional XANES [35]. Our results show that HERFD–XANES can be applied in a similar manner but with much greater accuracy than with conventional XANES, thanks to its higher spectral resolution and the fact that the background in the pre-edge and edge regions is significantly supressed when using the emission spectrometer. We estimate that the accuracy of the measured edge position is of the order of ± 0.1 eV.

In much the same way as HERFD–XANES, HERFD–EXAFS measurements are also possible using the XES spectrometer as is demonstrated in figure 9, showing that the EXAFS signal of $PrBr_2$ taken with the spectrometer overlaps with the spectrum taken in transmission mode, althought the noise level in the former is slightly higher.

It is important to note that EXAFS measurements using the spectrometer are limited due to the inherently low detection efficiency and only feasible for concentrated samples that can provide sufficient signal-to-noise over the wider energy range where the EXAFS oscillations are weak. In practical terms, it is usually more convenient to perform EXAFS measurements using conventional XAS.

There are however cases when the spectrometer can be used to overcome some of the main drawbacks of standard fluorescence measurements. For example, the capability of the spectrometer to separate fluorescence contributions that are very close together in energy, can be used for the study of samples containing additional elements with fluorescence emission lines that are very close in energy to those of the element of interest, and the latter is present only in relative low concentration. In those cases, conventional fluorescence XAS methods are not able to extract the structural information about the minority component, even when using energy discriminating detectors, as the resolving powder is insufficient to resolve the lines. In addition, HERFD–XAS can also be used to suppress diffraction peaks in XAS measurements of polycrystalline samples measured in fluorescence mode that otherwise distort the absorption spectrum.

3.2. Non-resonant x-ray emission spectroscopy

XES is performed by scanning the spectrometer over the emission line of interest while keeping the incident energy at a fixed value well above the absorption edge, typically between 100 and 200 eV.

The energy position and line shape of the emission lines provide information about the electronic configuration of the absorbing centre. For example, the shift in energy of the K_α emission lines has been used to determine the formal oxidation state of sulphur containing compounds [36], while the K_β lines have provided useful information regarding the spin state of Mn in GaN [37].

The K_β emission lines for two copper oxide samples are shown in figure 10. The measurements were taken using three Si(642) analyser crystals while maintaining the incident x-ray energy fixed at 9012 eV. Three analyser crystals were needed to maximise the efficiency of the spectrometer, as the K_β emission lines are significantly weaker than the K_α emission lines:
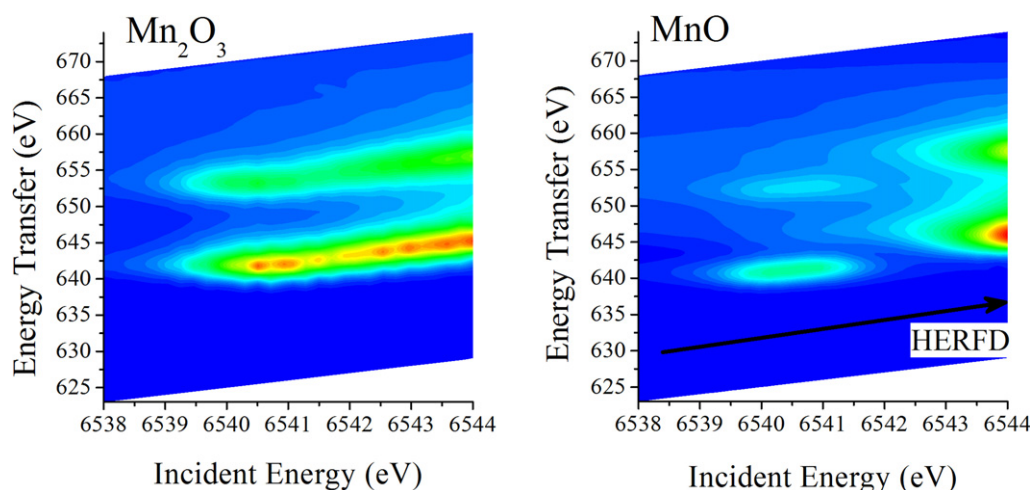
Figure 12. RXES maps for Mn_2O_3 and MnO_2. The intensity is scaled to the edge step. Slicing along the vertical axis of the above plots can provide *L*-edge like information.

for Cu, the $K_{\beta1,3}$ line is $\sim$17% of the $K_{\alpha1}$ line, and subsequently more challenging to measure. This is particularly true for the the very weak $K_{\beta2,5}$ and the K_{β}'' satellite line, often called valence to core (V2C) region, when long acquisition times are often needed to obtain a spectrum with a good enough signal-to-noise ratio. In the case of the copper oxides, we measured the V2C region separately to decrease the number of data points, and each set of measurements took approximately 3 h to record (six consecutive scans with 8 s per point acquisition time). We can see from figure 10 that the consistency of the spectra is excellent, thanks to the good stability of the spectrometer and detector, so the spectra can safely be merged to increase the signal quality.

V2C XES studies have become increasingly used in recent years as the technique provides a method to directly probe the valence levels of the absorbing centre. The V2C transitions arise from orbitals of mainly ligand character, making them very sensitive to the nature and the electronic structure of the coordinating ligand [38–42]. Figure 11 shows the V2C–XES for three chromium compounds. As can be seen in the figure, the position in energy of the satellite emission line moves towards higher energy when the coordinating ligand changes from C, to N and to O. This can be used to overcome one of the main limitations of conventional XAS: the inability to distinguish ligands that are neighbouring in the periodic table.

3.3. Resonant x-ray emission spectroscopy

In contrast with XES, when performing RXES, the incident energy is tuned to a resonant feature in the absorption edge. RXES measurements are usually taken at a variety of incident energies across the edge, producing two dimensional maps of the emission energy versus the incident energy. The maps are usually shown as the incident energy versus the transfer energy (figure 12), and a diagonal line through the RXES plane corresponds to a scan of the incident energy at fixed emission energy, e. g. to the HERFD–XANES spectrum. As shown in figure 12, by measuring the RXES map, additional information about intermediate states can be revealed.

RXES maps from two different manganese oxides have been collected to further demonstrate the potential of the I20 spectrometer, using three Si(422) analyser crystals. The obtained data are comparable with what has already been published in the literature [43]. In the case of the measured manganese oxide samples, the pre-edge region has been shown to reveal information on the upper-band excitations with energies much lower than the energy of the incident x-rays as the final state of RXES is equivalent to the *L*-edge excitation (2p3d^{n+1}).

4. Illustrative example

As an advanced illustrative example the Zn and Mn *K*-edge HERFD–XANES spectra of ZnO and MnO measured at the Zn and Mn $K_{\alpha1}$ emission line (2p$_{3/2}$−1s transition) are shown in figure 13, together with the spectrum collected from the same compound using conventional XAS in transmission detection mode. As expected, a clear resolution enhancement is observed: features A, C1, C2 and C3 in the ZnO and A1 and A2 in the MnO are better resolved in the HERFD–XANES, while others (B1 and D in ZnO and C and E1 in MnO) are simply not visible in the conventional XANES spectrum.

Ab initio calculations for the *K*-edge XANES in ZnO-wurtzite and MnO were carried out by using the multiple-scattering code CONTINUUM [44], based on the one-electron full-multiple-scattering theory [45]. In both cases, the XANES computations were performed for clusters including the contributions of neighbouring atoms within the first 8 Å around the photoabsorber and by using the Dirac-Hara exchange and correlation potential. No fitting parameters were used in the calculations. A complete discussion of the procedure can be found elsewhere [46, 47]. The results of the calculation are reported in figure 13, where different convolution values have been used to illustrate the effect of resolution broadening.

As can be seen in the figure, the computations performed show a very good agreement with the experimental results,
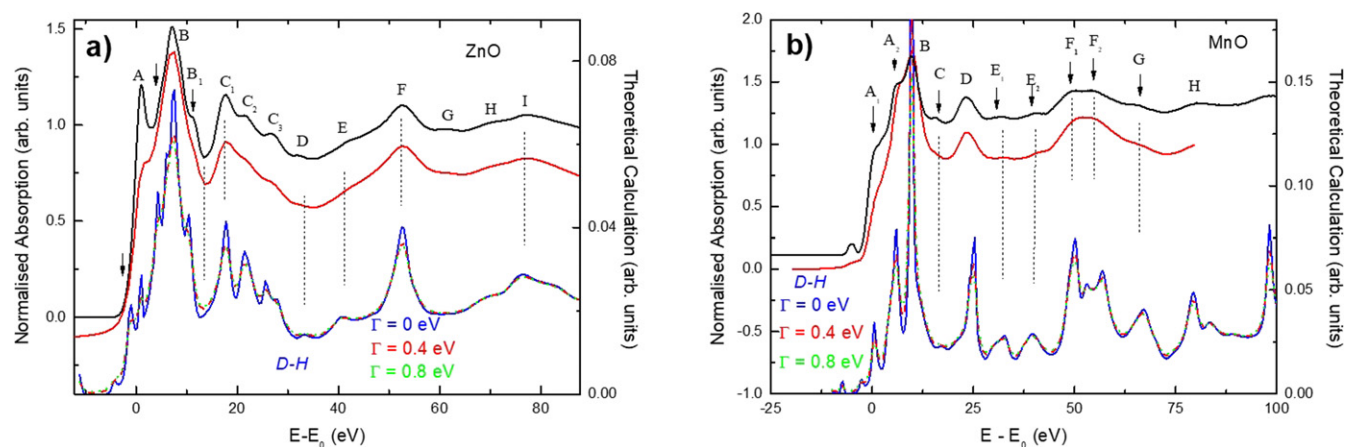
Figure 13. Comparison of the normalised HERFD–XANES (black line) and conventional XANES (red line) spectra for ZnO (panel (a)) and MnO (panel (b)), and the results of *ab initio* computations performed by using the multiple-scattering code CONTINUUM (see text for details).

both in the energy position and the relative intensity of the spectral features. It is important to highlight that the simulations reproduce remarkably well those features that are present in the HERFD–XANES experimental spectra but that are not visible or poorly defined in the conventional XANES spectra. This demonstrates the power of HERFD–XANES to enhance the experimental sensitivity of the spectroscopic method by overcoming the core-hole lifetime broadening, and shows how it can be used to better discriminate between various theoretical models.

5. Conclusions

An x-ray emission spectrometer has been successfully designed and commissioned for the I20-Scanning beamline at Diamond Light Source. The excellent energy stability and reproducibility of the spectrometer have been demonstrated by collecting three different types of measurements: (i) scanning the monochromator with the spectrometer at a fixed energy (HERFD–XANES); (ii) scanning the spectrometer with the monochromator at a fixed energy (XES) and (iii) scanning both the monochromator and the spectrometer (RXES maps). One of the key aims of this work was to develop a robust emission spectrometer that can be routinely operated by the user community and this goal has been achieved.

An upgrade of the spectrometer is currently under way. The new instrument will still be based on a 1 m diameter Rowland circle operating in the Johann configuration in the vertical plane, but the number of the analyser crystals will be increased from three to fourteen to greatly increase the efficiency of the instrument. To accommodate this large number of crystals, the spectrometer will be configured in two rows of seven analyser crystals each, and two 4e Medipix detectors will be used to maintain two independent Rowland circles. The use of two detectors will enable the option for collecting the photons selected by the 14 analyser crystals on different spots to avoid the saturation of the detectors. This will also enable the selection of the regions of the focal spot that offer the best possible energy resolution. This innovative design

will allow the spectrometer to operate in a two-colour mode with the possibility of measuring two emission lines simultaneously. The spectrometer will also be designed ground up to allow the pitch stages to be scanned in a coordinated manner to facilitate quick-scanning of the emission energy in approximately ± 20 eV range. These developments are expected to be available to the user community in 2023.

Data availability statement

The data that support the findings of this study are available upon reasonable request from the authors.

ORCID iDs

Sofia Diaz-Moreno https://orcid.org/0000-0001-7616-6515

References

[1] Bunker G 2010 *Introduction to XAFS: A Practical Guide to X-ray Absorption Fine Structure Spectroscopy* (Cambridge: Cambridge University Press)
[2] Filipponi A 2001 *J. Phys.: Condens. Matter.* **13** R23–60
[3] Evans J 2017 *X-ray Absorption Spectroscopy for the Chemical and Materials Sciences* (New York: Wiley)
[4] van Bokhoven J A and Lamberti C 2016 *X-ray Absorption and X-ray Emission Spectroscopy: Theory and Applications* (New York: Wiley)
[5] Glatzel P, de Groot F M F and Bergmann U 2009 *Synchrotron Radiat. News* **22** 12

[6] Glatzel P, Weng T-C, Kvashnina K, Swarbrick J, Sikora M, Gallo E, Smolentsev N and Mori R A 2013 *J. Electron Spectrosc. Relat. Phenom.* **188** 17

[7] Glatzel P and Bergmann U 2005 *Coord. Chem. Rev.* **249** 65

[8] Hämäläinen K, Siddons D P, Hastings J B and Berman L E 1991 *Phys. Rev. Lett.* **67** 2850

[9] Hazemann J-L *et al* 2009 *J. Synchrotron Radiat.* **16** 283

[10] Kleymenov E *et al* 2011 *Rev. Sci. Instrum.* **82** 065107

[11] Sokaras D *et al* 2013 *Rev. Sci. Instrum.* **84** 053102

[12] Kvashnina K O and Scheinost A C 2016 *J. Synchrotron Radiat.* **23** 836

[13] Duan P, Gu S, Cao H, Li J and Huang Y 2016 *X-ray Spectrom.* **46** 12

[14] Finkelstein K D, Pollock C J, Lyndaker A, Krawcyk T and Conrad J 2016 *AIP Conf. Proc.* **1741** 030009

[15] Moreti Sala M *et al* 2018 *J. Synchrotron Radiat.* **25** 580

[16] Ablett J M *et al* 2019 *J. Synchrotron Radiat.* **26** 1

[17] Glatzel P *et al* 2021 *J. Synchrotron Radiat.* **28** 362

[18] Klementiev K, Preda I, Carlson S, Sigfridsson K and Norén K 2016 *J. Phys.: Conf. Ser.* **712** 012018

[19] Szlachetko J *et al* 2012 *Rev. Sci. Instrum.* **83** 103105

[20] Alonso-Mori R *et al* 2012 *Rev. Sci. Instrum.* **83** 073114

[21] Johann H H 1931 *Z. Phys.* **69** 185

[22] Johansson T 1933 *Z. Phys.* **82** 507

[23] Hámos L v 1932 *Naturwissenschaften* **20** 705

[24] Diaz-Moreno S *et al* 2018 *J. Synchrotron Radiat.* **25** 998

[25] Hayama S *et al* 2018 *J. Synchrotron Radiat.* **25** 1556

[26] Collart E, Shukla A, Gélébart F, Morand M, Malgrange C, Bardou N, Madouri A and Pelouard J-L 2005 *J. Synchrotron Radiat.* **12** 473

[27] Bergmann U and Cramer S P 1998 *Proc. SPIE.* **3448** 198

[28] Plackett R, Horswell I, Gimenez E N, Marchal J, Omar D and Tartoni N 2013 *J. Instrum.* **8** C01038

[29] https://xrstech.com/

[30] Rovezzi M, Lapras C, Manceau A, Glatzel P and Verbeni R 2017 *Rev. Sci. Instrum.* **88** 013108

[31] Thompson A C 2009 *X-ray Data Booklet* (California: LBNL)

[32] Glatzel P, Smolentsev G and Bunker G 2009 *J. Phys.: Conf. Ser.* **190** 012046

[33] Chaboy J 2009 *J. Synchrotron Radiat.* **16** 533

[34] Farges F 2005 *Phys. Rev.* B **71** 155109

[35] Zaharieva I *et al* 2009 *J. Phys.: Conf. Ser.* **190** 012142

[36] Devillers T *et al* 2012 *Sci. Rep.* **2** 722

[37] Alonso Mori R, Paris E, Giuli G, Eeckhout S G, Kavčič M, Žitnik M, Bučar K, Pettersson L G M and Glatzel P 2009 *Anal. Chem.* **81** 6516

[38] Pollock C J and DeBeer S 2011 *J. Am. Chem. Soc.* **133** 5594

[39] Bauer M 2014 13827 *Phys. Chem. Chem. Phys.* **16** 13827–37

[40] Rovezzi M and Glatzel P 2014 *Semicond. Sci. Technol.* **29** 023002

[41] Pollock C J and DeBeer S 2015 *Acc. Chem. Res.* **48** 2967

[42] Cutsail G E, Gagnon N L, Spaeth A D, Tolman W B and DeBeer S 2019 *Angew. Chem., Int. Ed.* **58** 9114

[43] Glatzel P *et al* 2004 *J. Am. Chem. Soc.* **126** 9946

[44] Natoli C R, Misemer D K, Doniach S and Kutzler F W 1980 *Phys. Rev.* A **22** 1104

[45] Natoli C R and Benfatto M 1986 *J. Phys. Colloques* **47** C8

[46] Guglieri C and Chaboy J 2010 *J. Phys. Chem* C **114** 19629

[47] Guglieri C, Céspedes E, Prieto C and Chaboy J 2011 *J. Phys.: Condens. Matter.* **23** 206006

[48] Ravel B and Newville M 2005 *J. Synchrotron Radiat.* **12** 537